Development of a Permanent Magnet Claw Pole Motor with Soft Magnetic Composite Core

Y.G. Guo*, J.G. Zhu*, P.A. Watterson* and W. Wu**

*Faculty of Engineering, University of Technology, Sydney, P.O. Box 123, Broadway, NSW 2007, Australia
**CSIRO Telecommunications and Industrial Physics, P.O. Box 218, Lindfield, NSW 2070, Australia

SUMMARY: *This paper reports the development of a three-phase permanent magnet claw pole motor with soft magnetic composite stator, taking advantage of the unique properties of the material. Advanced design and performance analysis methods were employed, such as the three-dimensional finite element analysis of magnetic fields for parameter calculation and dimension optimisation, rotational core loss models combined with finite element method for core loss prediction, and hybrid thermal model with distributed heat sources for the temperature rise calculation, etc. The design and analyse methods are validated by experiment on the prototype driven by a brushless DC drive scheme.*

1 INTRODUCTION

The new soft magnetic composite (SMC) materials produced by powder metallurgy techniques have undergone significant development in the past few years because of their unique properties and potential application in electrical machines.[1,2] This type of material is made of iron powder of high purity and compressibility. The particles are bonded with a coating of an organic material, which produces high electrical resistivity. The coated powder is then pressed into solid material using a die and finally heat treated to anneal and cure the bond.

Compared with electrical steels widely used in rotating machines and transformers, the major advantage of the SMC material is the prospect of large volume manufacturing of low cost electromagnetic devices. Because the iron cores and parts can be pressed in a die into the desired shape and dimension, the further machining is minimised and hence the production cost is greatly reduced. In addition, the powdered nature of the material yields lower eddy current losses and isotropic magnetic properties. Therefore, it is very suitable for specially structured, such as claw pole, motors with three-dimensional (3D) fluxes. The permeability of this material, however, is lower than that of electrical steels. It is expected that this material would be appropriate for construction of permanent magnet (PM) motors for which the magnetic reluctance of the magnet dominates the magnetic circuit, making such motors less sensitive to the permeability of the core than armature magnetised machines, e.g. induction and reluctance machines.

Since the iron particles are insulated by the surface coating and adhesive, which is used for composite bonding, the eddy current loss is much lower than that in laminated steels, especially at higher frequencies. The total loss is dominated by hysteresis loss, which is higher than that of laminated steels due to the particle deformation during compaction. This property implies SMC motors to better operated at higher frequencies, resulting in reduced machine size and weight.

This paper presents the design, performance analysis, prototype construction and experiment of a 3-phase 3-stack PM claw pole motor with an SMC stator. SOMALOY™ 500, a new soft magnetic composite produced by Höganäs AB, Sweden, is used as the stator core material. It is characterised by a thin continuous surface insulation layer with little or no effect on the powder compressibility. The unique properties of SMC are taken into account in the motor design.

The major motor parameters are calculated based on the magnetic field distribution through 3D finite element method (FEM). Rotational core losses of SOMALOY™ 500 with rotating magnetic fluxes at different frequencies were measured using a single sheet rotational core loss tester and applied in the performance calculation.[3,4] The motor performance is predicted by an equivalent circuit under the optimum brushless DC control condition.

The initial design and analysis about this three-phase PM claw pole motor with SMC core were reported in our previous work[5,6], but this paper presents a thorough picture of the development of the SMC prototype and adds more updated theoretical and experiment results.

2 STRUCTURE AND DIMENSIONS

Due to the nearly universal use in automobile alternators, electrical machines with claw pole rotors have been manufactured in mass production for many years. These machines have quite simple excitation coil and pole systems producing the excitation magnetic

fields. They are capable of producing torque densities up to three times greater than the conventional machines because their topology allows the pole number to be increased without reducing the magnetomotive force per pole. The excessive eddy currents in the commonly used solid steel core, however, limit the motors to very small sizes and/or low speeds and result in low efficiency.

Because of the complex structure, it is very difficult to construct the claw poles using lamination steels. SMC offers an opportunity to overcome these problems.

Figure 1 illustrates the magnetically relevant parts of the rotor and the stator of the prototype. Table 1 lists the dimensions and major parameters. The three phases of the motor are stacked axially with an angular shift of 120° electrical from each other. Each stator phase has a single coil (not shown in the figure) around an SMC core, which is moulded in two halves. The outer rotor comprises a tube of mild steel with an array of magnets for each phase mounted on the inner surface. Mild steel is used for the rotor because the flux density in the yoke is almost constant.

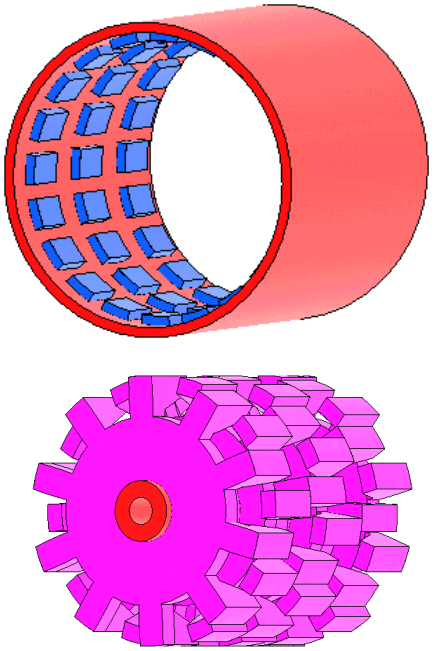

Figure 1: Magnetically relevant parts of the claw pole motor

For the prototype, the motor size and core geometry were to a large extent determined by the dimensions of the available SOMALOY™ 500 preforms. They were chosen the same as those of a PM SMC transverse flux motor prototype, enabling comparison.[7] A pole number of 20 was chosen giving an operating frequency of 300 Hz at 1800 rpm. It is not an unrealistically high frequency to work at for SMC materials. Since a simple concentrated stator winding is used, a reasonably high fill factor can be achieved and the manufacturing cost can be very low.

Table 1
Dimensions and major parameters

Dimensions and parameters	Quantities
Rated frequency (Hz)	300
Number of phases	3
Rated power (W)	500
Rated line-to-neutral voltage (V)	64
Rated phase current (A)	4.1
Rated speed (rev/min)	1800
Rated torque (Nm)	2.65
Rated efficiency (%)	81
Rated temperature rise (°C)	75
Number of poles	20
Stator core material	SOMALOY™ 500
Stator outer radius (mm)	40
Effective stator axial length (mm)	93
Rotor outer radius (mm)	47
Rotor inner radius (mm)	41
Permanent magnets	NdFeB, Grade N30M
Number of magnets	60
Magnet dimensions	OD88 x ID82 x 15 mm arc 12°
Magnetisation directions	Radially outward and inward
Main airgap length (mm)	1
Sub-airgap length* (mm)	4.2
Stator shaft material	Mild steel
Shaft outer radius (mm)	9
Number of coils	3
Coil window dimension (mm^2)	17 x 11
Number of turns	75
Number of strands	2
Diameter of copper wire (mm)	0.71
Resistance per phase at 115°C (Ω)	0.302

* The sub-airgap is defined as the gap between the sides of the claw poles of the two separated pieces.

3 3D MAGNETIC FIELD ANALYSIS

The magnetic circuits of three stacks (or phases) of the motor are basically independent. For each stack, because of the symmetrical structure, it is only required to analyse the magnetic field in one pole pitch, as shown in figure 2.

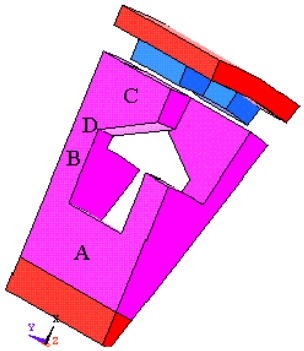

Figure 2: Region for field solution

At the two radial boundary planes of one pole pitch, the magnetic scalar potential obeys the so-called

half-periodical boundary conditions:

$$\varphi_m(r, \Delta\theta/2, z) = -\varphi_m(r, -\Delta\theta/2, -z) \quad (1)$$

where $\Delta\theta = 18^o$ is the angle of one pole pitch.

3.1 Magnetic flux linking the stator winding at no-load

As the rotor rotates, the flux linking the stator winding varies and an electromotive force (*EMF*) is induced. The *EMF* frequency depends on the rotor speed, while its waveform is determined by the waveform of the flux. At no-load, the flux waveform was calculated by rotating the rotor for one pole pitch in 12 steps. As plotted in figure 3, this flux waveform versus the rotor position is almost perfectly sinusoidal. In the design, the motor structure and dimensions have been adjusted such that the peak flux linkage of the stator winding is the maximum.

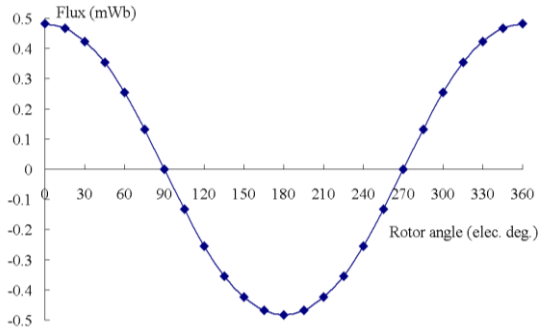

Figure 3: No-load flux per turn of a phase winding

3.2 Cogging torque

Cogging torque is caused by the tendency of the rotor to line up with the stator in a particular direction where the magnetic circuit has the highest permeance. The cogging torque arises from the reluctance variation of the magnetic circuit as the rotor rotates and exists even when there is no stator current. Figure 4 shows the cogging torque versus the rotor position for one phase of the machine, calculated by the Coulomb virtual work method. This curve was calculated by rotating the rotor for one pole pitch in 12 steps, i.e. 15° electrical or 1.5° mechanical per step.

The cogging torque has a period of 180 electrical degrees and anti-symmetry about zero, hence only even sine harmonics, which were computed by the discrete Fourier transformation method to be

$$T_A \approx 0.6150\sin 2\theta + 0.0629\sin 4\theta - 0.1270\sin 6\theta - 0.0479\sin 8\theta + 0.0030\sin 10\theta + 0.0001\sin 12\theta \quad (2)$$

where θ is the rotor angle in electrical degrees. The stator claw pole teeth on the three phases are shifted by 120 electrical degrees, and all even harmonics other than order 6 or its multiples sum to zero over the three phases. The magnitudes of the 6th and 12th harmonics of cogging torque are 0.3810 Nm and 0.0003 Nm, respectively.

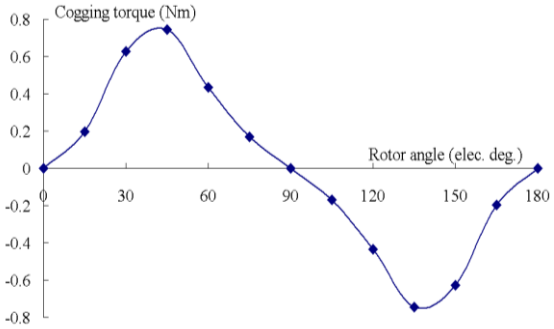

Figure 4: Cogging torque versus rotor position for one stack

3.3 Inductance and armature reaction

The self-inductance of each phase winding can be calculated by

$$L_1 = \frac{N_1\phi_1}{I_1} \quad (3)$$

where ϕ_1 is the magnitude of the flux linking the stator winding due to a stator current I_1 in each of N_1 turns. It can be obtained from the results of a field analysis with a stator current I_1 while the permanent magnets are "switched off", i.e. remanence is set to zero. In this three-phase motor, the mutual inductance between phase windings can be considered as zero since the magnetic circuit for each phase is basically independent. From table 2, it can be seen that the per-turn inductance is very uniform against rotor angles. The inductance scales as N_1^2 and so is 5.24 mH for 75 turns. It is also shown in table 2 that the armature reaction for the rated current is quite small and it will not demagnetise the magnets.

Table 2
Inductance and armature reaction in magnets

Rotor position (elec. deg.)	Self inductance per turn (μH)	Maximum B in magnets (T)
0	0.932	0.031
45	0.932	0.030
90	0.932	0.037

3.4 Core loss calculation

The core loss is caused not only by alternating but also by rotational magnetic fields, and should be considered properly in the design.[8] In claw pole machines, the armature carries significant fluxes in all directions. Due to the 3D nature of magnetic fields, the flux density locus at one position can be alternating with or without harmonics, two-dimensional or even 3D rotating with

purely circular or elliptical patterns. Figure 5 illustrates the calculated 3D flux density locus in a typical element of claw pole (point C of figure 2), showing that the flux density in the claw pole is truly 3D and rotating elliptically.

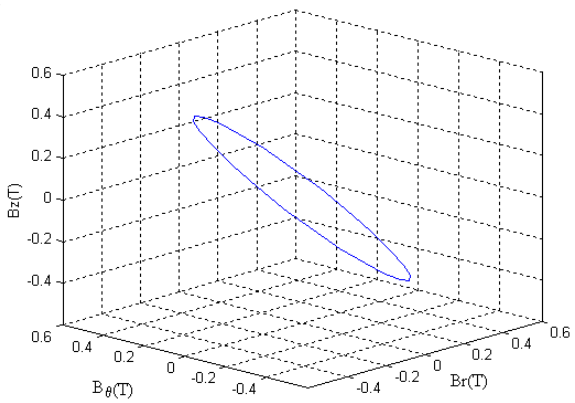

Figure 5: Flux density locus in a typical element of the claw pole

An improved method is applied for predicting core losses in the 3D-flux SMC machine.[4] Different formulations are used for core loss prediction with purely alternating, purely circular rotating, and elliptically rotating flux density vectors, respectively. A series of 3D finite element analyses are conducted to determine the flux density locus in each element when the rotor rotates (an example is shown in figure 5). The calculated and the measured core losses of the motor at different speeds at no-load are plotted in figure 6. It can be seen that the theory agrees well with the experiment.

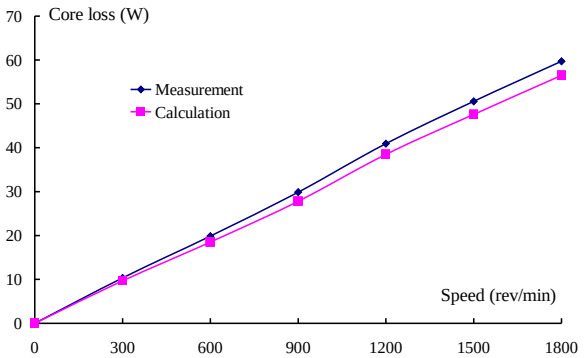

Figure 6: Core loss calculation and measurement at no-load

Core losses do occur in the magnets and the rotor yoke due to the ripples of flux density when the rotor rotates. However, the numerical results of FEA of the magnetic field have shown that the flux density vectors in the magnets and the rotor yoke are nearly constant and the ripples are negligible. Therefore, only the power loss in the SMC stator core was computed.

Under load operation, the magnetic field in the core is produced by not only the rotor magnets, but also the stator current, which can be very different from that at no-load. The calculation of core loss with load uses the similar procedure as for calculating the no-load core loss, except that the magnetic field analysis was conducted with both the stator current and PM excitations.

3.5 Optimisation of magnet length

Taking advantage of the isotropic magnetic property of SMC material, the magnet length can be chosen longer than the claw pole to obtain higher stator flux and hence higher specific torque. However, too much magnet overhang may lead to saturation and is cost-ineffective. Comparing the ratio of torque to overall material cost, the magnet length is chosen as 15 mm, which exceeds the claw pole head by 1.65 mm.

3.6 Flux penetration in stator shaft

In the field analysis, the flux is assumed not to pass through the stator shaft since the mild steel shaft has much higher conductivity and permeability than the SMC yoke, as shown in table 3.

Table 3
Comparison of SMC and mild steel

Parameters	SMC	Mild steel
Relative permeability	130	5000 (range 1500 –10000)
Conductivity (S/m)	500 - 10000	1.12×10^7
Penetration or skin depth at 300 Hz (mm)	25.5 – 114	0.123

The penetration or skin depth can be calculated by

$$\delta = \sqrt{\frac{2}{\omega\mu\sigma}} \tag{4}$$

where μ is the magnetic permeability of the material, σ the electrical conductivity, and ω the angular frequency of the flux. Assuming linear permeability, the flux penetrating the shaft and the eddy current loss are given by,[9]

$$\phi = B_p(2\pi r_{shaft})\frac{\delta}{\sqrt{2}} \tag{5}$$

$$w_e = \frac{B_p^{\,2}}{2\mu^2\sigma\delta}(2\pi r_{shaft} l_{shaft}) \tag{6}$$

where B_P is the peak flux density just inside the shaft surface, r_{shaft} is the shaft radius, and l_{shaft} is the effective shaft length. The maximum flux density in the stator yoke is about 1.0 T, kept low to reduce core loss. By continuity of tangential magnetic field strength, B_P will be saturated, around 2 T. Though (5) and (6) are for

non-saturated material, if applied they give that the penetrating flux and eddy current loss in the mild steel shaft at 300 Hz are only 0.007 mWb and 0.096 W, respectively. Compared to the flux and core loss in the SMC yoke, these values are negligible.

3.7 Eddy current in SMC

Since it is very difficult to model the complex cyclic magnetisation of SMC in the FEM magnetic field analysis, a single valued B-H curve is used instead and iron loss is then estimated as a post-processor exercise. This approach may have a risk in calculating eddy current.[2] The insulation between grains in SMC is not perfect and significant bulk eddy current, which flows between grains, may well be present. The ratio of the material dimensions to skin depth is a critical parameter. If the smallest dimension of the component normal to the magnetic field plane is near the skin depth the field will be significantly disturbed by the eddy currents and will be restricted to near the surface of the component. The result is that the effective permeability falls, a phase shift is introduced, high loss is induced, and the skin effect must be part of the analysis, which is far more complex.

The narrowest dimensions for the SMC claw pole teeth, claw pole discs and the stator yoke are 5 mm, 7 mm and 10 mm, respectively. They are much smaller than the skin depth at the rated frequency, as in table 3. Thus, the magnetic field analysis can be conducted ignoring eddy currents.

4 PERFORMANCE CALCULATION

The motor uses a standard six-transistor bridge drive circuit. With open-loop control, the motor can operate in normal synchronous mode. With the closed-loop control of position feedback it can also operate in brushless DC mode where the current I_1 and the induced *EMF*, E_1 in the stator winding are in phase, to achieve a maximum electromagnetic power P_{em} at a given speed, i.e.

$$P_{em} = 3E_1 I_1 \tag{7}$$

The induced stator *EMF* can be determined by

$$E_1 = \frac{\omega_1 N_1 \phi_m}{\sqrt{2}} \tag{8}$$

where $\omega_1=2\pi f_1$ is the angular rotor speed in electrical radians per second, f_1 the frequency of the induced stator *EMF* in Hertz, N_1 the number of turns of the stator winding, and ϕ_m the magnitude of the magnetic flux linking the stator winding due to the permanent magnets.

The rated line-to-neutral rms voltage is calculated by:

$$V_1 = \sqrt{(E_1 + I_1 R_1)^2 + (I_1 X_1)^2} \tag{9}$$

where R_1 is the resistance of one phase winding and X_1 is the reactance. At 1800 rpm (300Hz), E_1= 48.9 V, and for a rated current of 4.1 A, limited by the temperature rise of the stator winding, P_{em}=601.5 W and V_1=64.5 V. The corresponding DC input voltage of the inverter can be estimated by[9]

$$V_{dc} = 2.34 V_1 \tag{10}$$

The output power, output torque, input power, and efficiency are calculated by

$$P_{out} = P_{em} - P_{Fe} - P_{mec} \tag{11}$$

$$T_{out} = P_{out} / \omega_r \tag{12}$$

$$P_{in} = P_{em} + P_{cu} \tag{13}$$

$$P_{cu} = 3 I_1^2 R_1 \tag{14}$$

$$\eta = P_{out} / P_{in} \tag{15}$$

where P_{Fe} is the core loss, P_{mec} the mechanical loss including windage and friction, P_{cu} the copper loss, and ω_r the angular speed. The mechanical loss was estimated by 1%*P_{em}, which was validated by the "dummy stator test". At the rated operation, the efficiency is calculated as 81.5%.

At a given voltage input, the steady state characteristic with optimum feedback can be predicted by

$$\omega_r = \frac{V_1}{K_e} - \frac{R_1}{K_e K_T} T_{em} \tag{16}$$

where K_e is the back *EMF* constant, K_T the torque constant, and T_{em} is the electromagnetic torque.

5 THERMAL ANALYSIS

To obtain an economic utilisation of the materials and safe operation of the motor it is necessary to predict with reasonable accuracy the temperature rise of the internal parts, especially in the coils and magnets. In this paper, the temperature rise is calculated by using a hybrid thermal network with distributed heat sources as shown in figure 7. For higher computation accuracy, any part, e.g. the airgap and claw pole, can be divided into as many small segments as possible.

The conduction resistances in the following sections are calculated: rotor yoke (R_{ry}), magnets (R_m), glue between magnet and rotor yoke (R_{mg}), air gap (R_{ag}), stator yoke (R_{Fe1}), stator claw pole discs (R_{Fe2}), stator claw poles (R_{Fe3}), varnished copper wire (R_{cu}) and insulations (R_{I1}, R_{I2}, R_{I3}) between the winding and the stator claw pole disc, the stator shaft and the air gap, respectively. In addition, the thermal resistances of the stator shaft (R_{ss}), the aluminum end plates (R_{al}) and the stationary air (R_{sa}) between the claw pole discs and the end plates are calculated separately.

The equivalent thermal resistances to the heat convection (radiation in motor thermal analysis is usually ignored) of the following sections are calculated: between claw pole surface and inner air in the airgap (R_{FeA}), between winding and inner air (R_{WA}), between magnet and inner air (R_{mA}), between rotor yoke and inner air (R_{ryA1}), and between rotor yoke and outer air (R_{ryA2}).

The heat sources are the stator coil copper losses (P_{cu}), the stator core losses (P_{Fe}), and the mechanical losses due to windage and friction (P_{mec}). The improved method for core loss calculation can obtain the loss distribution, which is a great advantage for the thermal calculation by the hybrid thermal model.

The temperature rises at the middle points of several parts are calculated as 74 °C in the coil, 77 °C in the stator core, 55 °C in the air gap, 45 °C in the magnets, and 22 °C on the rotor yoke outer surface.

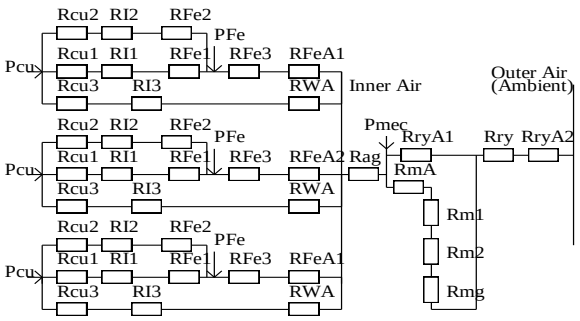

Figure 7: A schematic diagram of thermal network

6 EXPERIMENT VALIDATION

Figure 8 shows the setup of the 3-phase 3-stack claw pole PM motor with SMC stator core (on the right). A DC machine (on the left) is connected via a torque transducer (in the middle) as the load when the prototype operates as a motor, or the driver when the prototype operates as a generator.

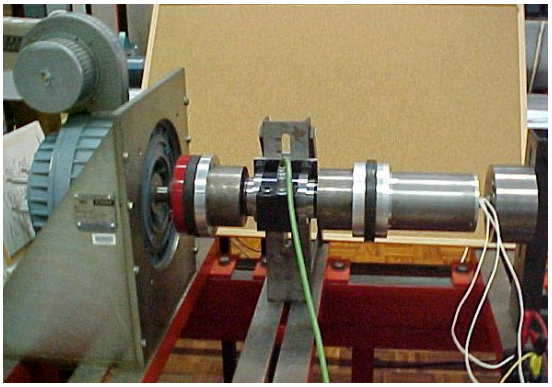

Figure 8: Test setup of a claw pole PM SMC motor

6.1 Measurement of resistance and inductance

When a DC current I_{dc} of 1 A is fed through the stator winding, the voltage V_{dc} across the winding is measured and then the resistance can be calculated by

$$R_1 = V_{dc} / I_{dc} \tag{17}$$

When an AC voltage V_{ac} with frequency f_1 is applied across the stator winding, the current flowing through the winding I_{ac} is measured and then the inductance can be calculated by

$$L_1 = \frac{\sqrt{(V_{ac} / I_{ac})^2 - R_1^2}}{2\pi f_1} \tag{18}$$

The measured phase resistance is 0.225 Ω at room temperature or 0.3 Ω at 115 °C, and the measured phase inductance is 5.79 mH. The measurements match the prediction.

6.2 Measurement of cogging torque

For the measurement of cogging torque, the stator is mounted on a rotatable air-bearing plate with very little mechanical friction. By displacing the stator with the rotor fixed, the cogging torque was measured and plotted in figure 9. It substantially matches the theoretical calculation.

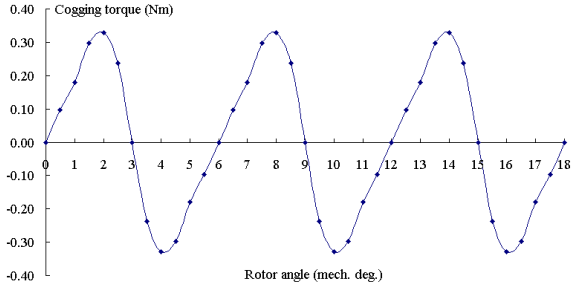

Figure 9: Measured cogging torque of the claw pole motor

6.3 Back EMF waveform

When the prototype operates as a generator, driven by the DC machine, the back electromotive force can be measured from the open circuit voltage. Figure 10 shows the measured *EMF* waveforms, which are very close to sinusoidal. The waveforms of three phases are with the same magnitude but shifted each other by 120 electrical degrees in phase angles.

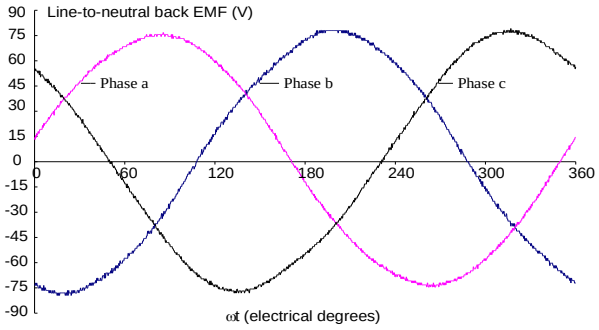

Figure 10: Measured back EMF waveforms at 1800 rpm

6.4 Steady state characteristics

The steady state characteristics were measured with different loads at a fixed inverter DC link voltage. The load was varied by changing the electrical output of the DC generator. Figure 11 shows the mechanical characteristics with different fixed DC link voltages, namely the relationship of the speed against the output torque. The rated characteristic is the curve on the top with an inverter voltage of 165 V. The motor has successfully operated with the rated torque and speed for a long time. The audible noise is quite low.

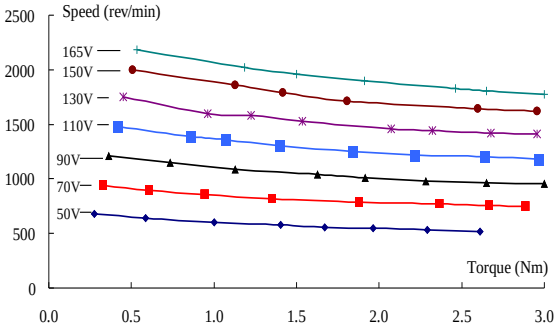

Figure 11: Curves of the speed against output torque with different DC link voltages

The curves of the stator currents against the output torque are illustrated in figure 12, and the variations of the input power, output power and efficiency are shown in figure 13. The inverter input DC current and the motor phase AC current become closer when the load increases, and the ratio ranges from 1.0 to 1.28. The motor reaches the highest efficiency, 81.0% at the rated output torque, 2.65 Nm.

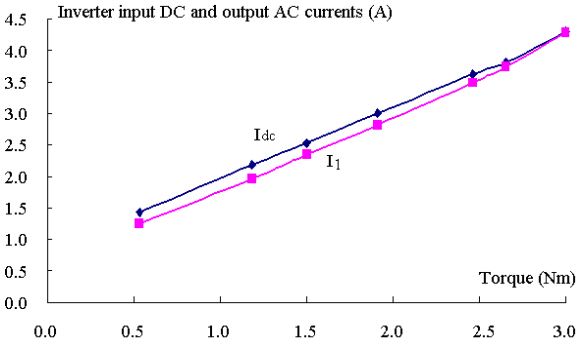

Figure 12: Inverter DC input and AC output currents against output torque

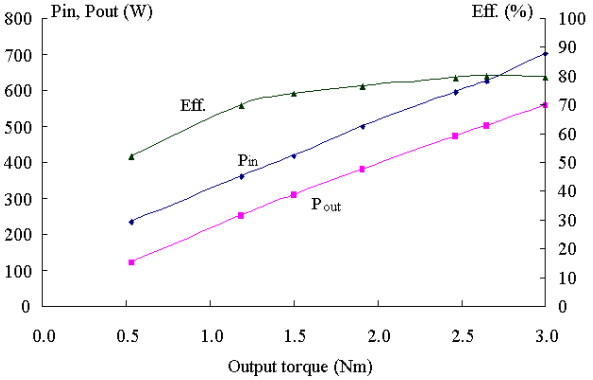

Figure 13: Curves of inverter input power, motor output power and efficiency versus output torque

6.5 No-load core loss measurement

The no-load core loss is measured by separating the core loss from the mechanical loss using the dummy stator method, which includes two measurements. In the first measurement, the prototype is driven by the DC motor on the left and the power fed into the DC motor is measured. The second measurement is conducted while the SMC stator of the prototype is replaced by a wood tube.

The difference between the readings of electromagnetic power for the two cases gives the core loss, as illustrated in figure 6. Here, we assumed the core loss and mechanical loss of the DC driving motor are constant at certain rotor speed. The dummy stator is used to simulate the windage. The prototype is assumed to have the same windage and friction loss for the SMC stator and the dummy stator if it is driven at the same speed.

6.6 Measurement of temperature rise

The winding temperature can be measured on-line by the buried thermocouples. When the prototype has been run at the full load for half an hour, the temperature reading becomes stable. The stator coil temperature was measured as 91 ^{o}C with an ambient

temperature of 20 ^{o}C (or 71 ^{o}C temperature rise). The rotor yoke surface temperature was measured to be 43 ^{o}C by an infrared temperature probe (or 23 ^{o}C temperature rise). These agree with the previous calculated values well.

7 COMPARISON WITH LAMINATED MOTOR

Since it givens the rated performance of 500 W output, 1800 rpm, 81.5% efficency, the designed claw pole SMC motor with outer diameter (OD) of 94 mm and an axial length (excluding shaft) of 137 mm compares favourably with other laminated motors. For example, an aluminum TEFV induction motor rated 370 W at 1380 rpm, which is about the same torque (3% lower), has an efficiency of only 73% from frame size D71G, with an OD of 126 mm including fins and total length of 220 mm (including fan but excluding shaft).[11] The claw pole SMC motor has similar performance from a smaller volume compared to this commercial motor.

8 CONCLUSION

To investigate the potential of SMC materials in manufacturing of small motors of complex structures, a 3-phase PM claw pole motor with SMC core has been designed and manufactured. The prototype performance is comparable to that of similar motors with electrical steel cores at potentially reduced manufacturing cost. The method for the motor design and performance analysis has been validated by the experiment on the motor.

REFERENCES

[1] The latest development in soft magnetic composite technology. SMC Update, Reports of Höganäs AB, Sweden, 1997-2003. Available at http://www.hoganas.com/, see News then SMC Update.

[2] Jansson P, Jack AG. Magnetic assessment of SMC materials. Proc of 21st Annual Conference on Properties and Applications of Magnetic Materials, Chicago, USA, May 2002:1-9.

[3] Zhu JG, Zhong JJ, Ramsden VS, Guo YG. Power losses of composite soft magnetic materials under two dimensional excitations. Journal of Applied Physics, April 1999; 85(8):4403-4405.

[4] Guo YG, Zhu JG, Zhong JJ, Watterson PA, Wu W. An improved method for predicting magnetic power losses in SMC electrical machines. Int Journal of Applied Electromagnetics and Mechanics, 2004;19(1-4):75-78.

[5] Guo YG, Zhu JG, Watterson PA, Wu W. Design and analysis of a three-phase three-stack claw pole permanent magnet motor with soft magnetic composite core. Proc of Australasian Universities Power Engineering Conference, Christchurch, New Zealand, 28 September - 1 October 2003; paper no. 85.

[6] Guo YG, Zhu JG, Watterson PA, Holliday WM, Wu W. Improved design and performance analysis of a claw pole permanent magnet SMC motor with sensorless brushless DC drive. Proc of the 5th IEEE Int Conf on Power Electronics and Drive Systems, Singapore, 17-20 November 2003:704-709.

[7] Guo YG, Zhu JG, Watterson PA, Wu W. Design and analysis of a transverse flux machine with soft magnetic composite core. Proc of the 6th Int Conf on Electrical Machines and Systems, Beijing, China, 9-11 August 2003:153-157.

[8] Guo YG, Zhu JG, Zhong JJ, Wu W. Core losses in claw pole permanent magnet machines with soft magnetic composite stators. IEEE Transactions on Magnetics, September 2003;39(5):3199-3201.

[9] Carter GW. The electromagnetic field in its engineering aspects. 2nd Edition, Longmans, London, 1967:243-247.

[10] Watterson PA. Analysis of six-step 120^{o} conduction permanent magnet drives. Proc of Australasian Universities Power Engineering Conference, Sydney, Australia, 28 September - 1 October 1997:13-18.

[11] Aluminum IP54 motors. Brook Crompton Catalogue 1X1800, July 1991.

Figure 1: Magnetically relevant parts of the claw pole motor

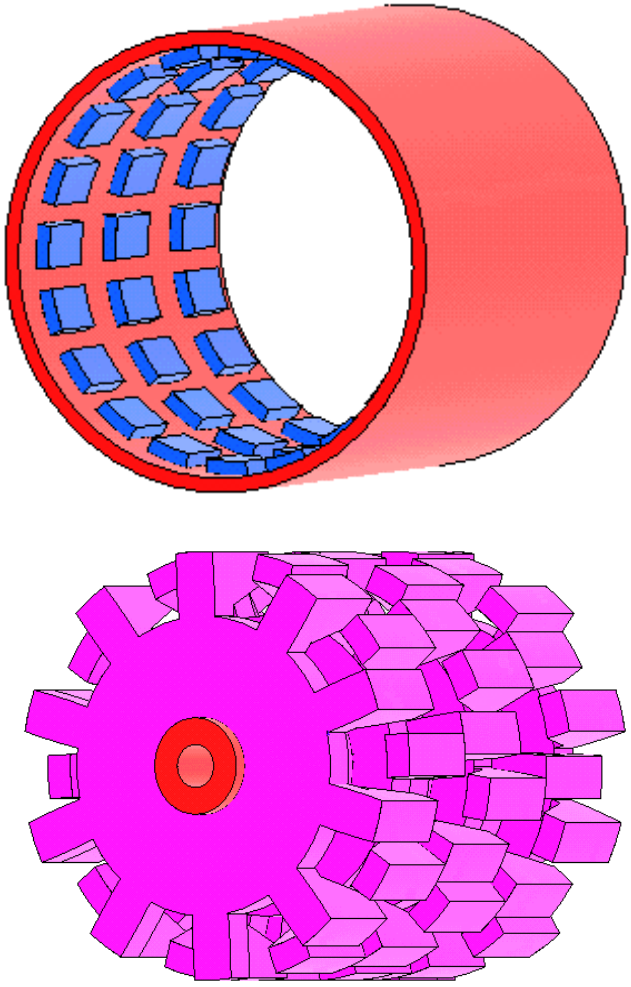

Figure 2: Region for field solution

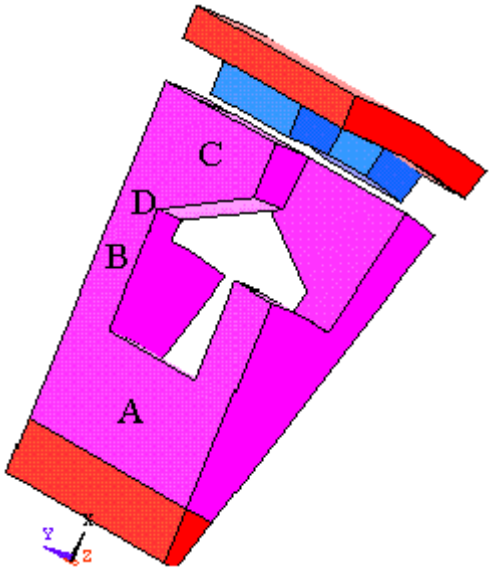

Figure 3: No-load flux per turn of a phase winding

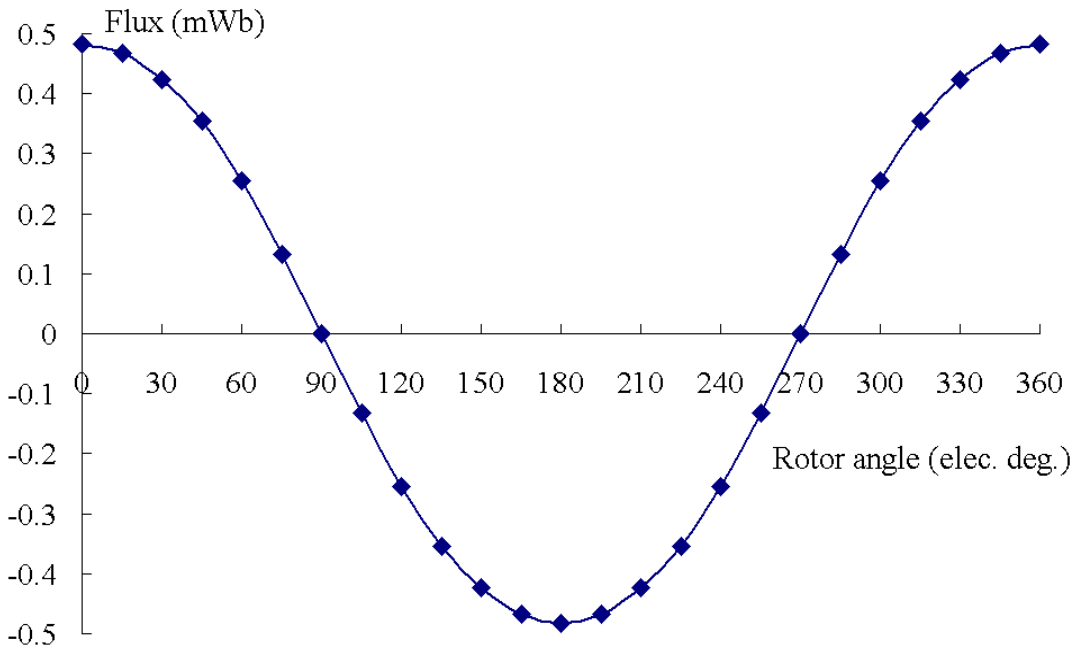

Figure 4: Cogging torque versus rotor position for one stack

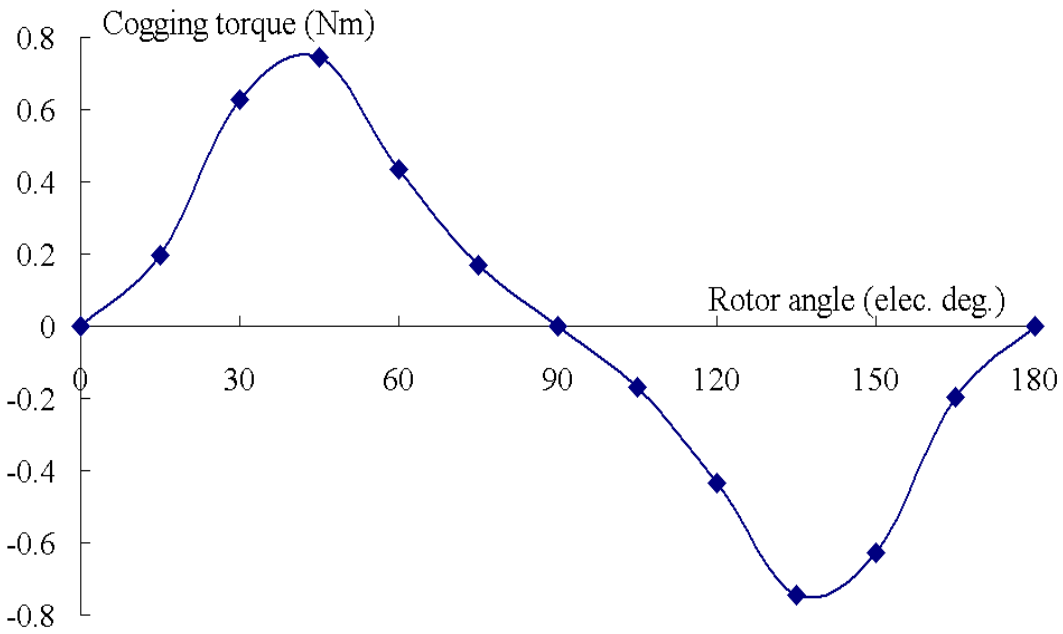

Figure 5: Flux density locus in a typical element of the claw pole

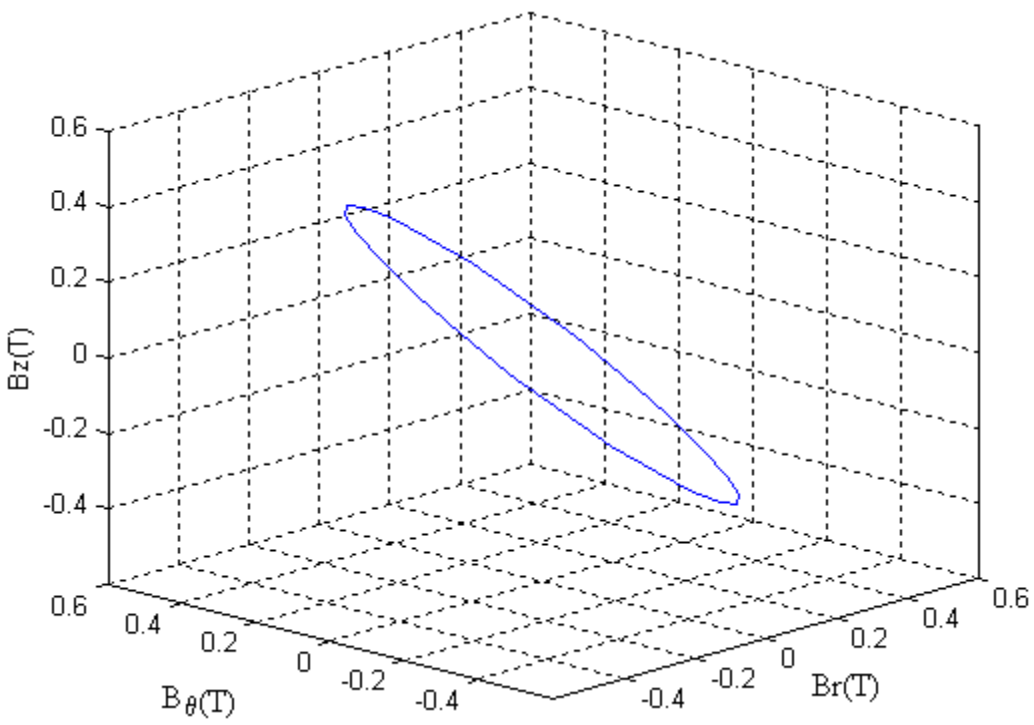

Figure 6: Core loss calculation and measurement at no-load

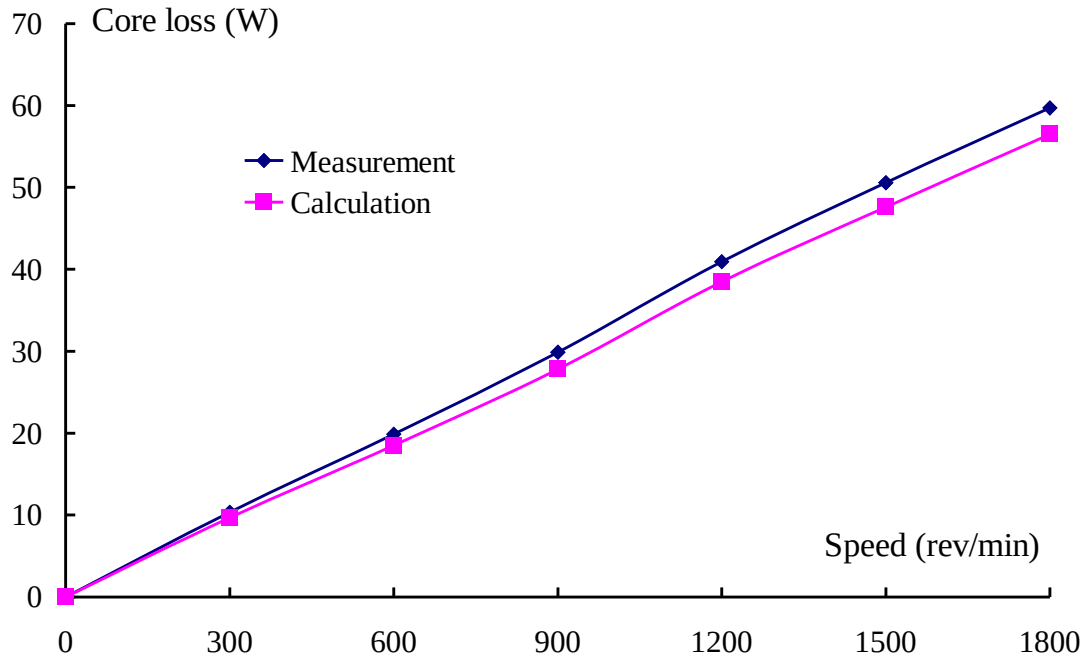

Figure 7: A schematic diagram of thermal network

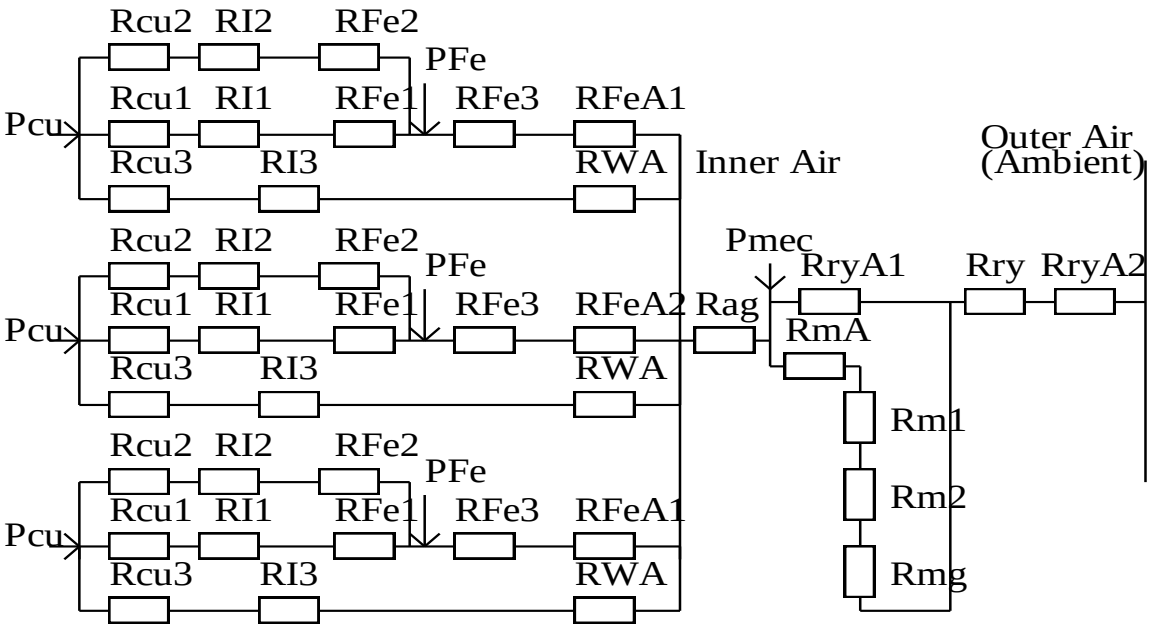

Figure 8: Test setup of a claw pole PM SMC motor

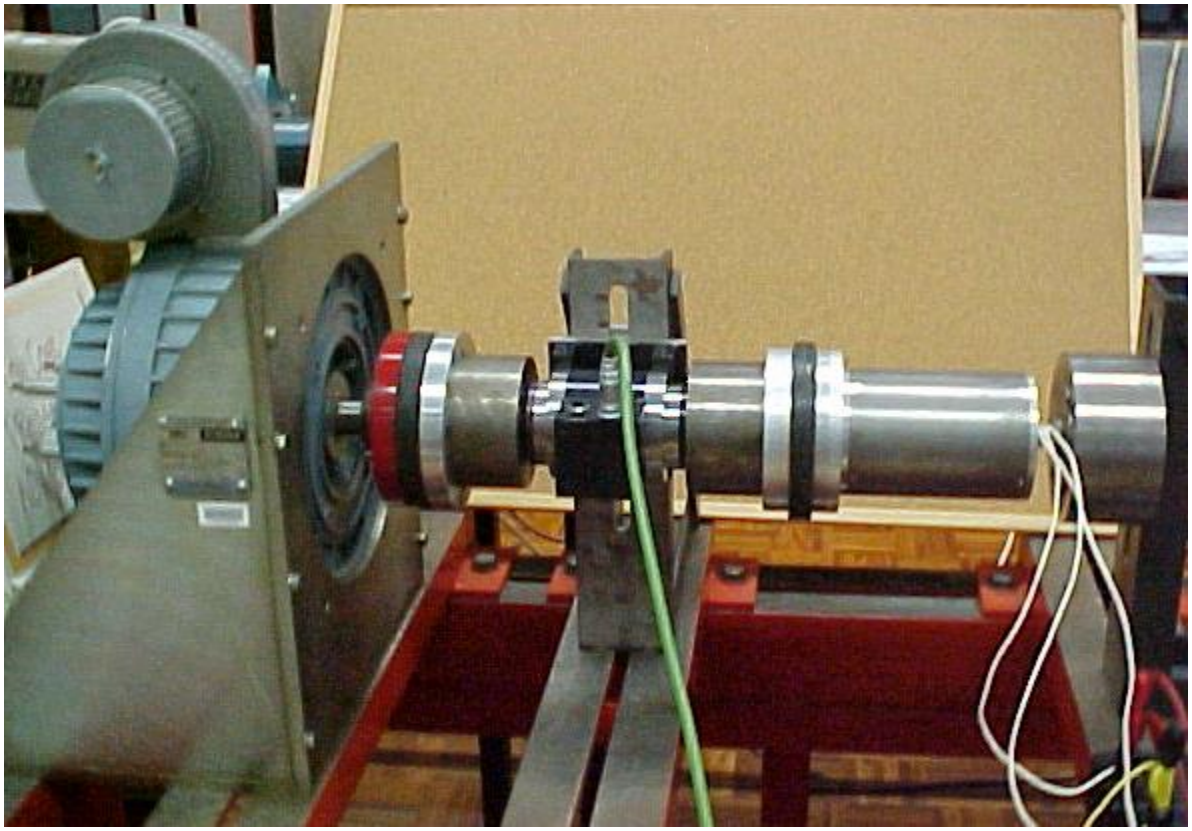

Figure 9: Measured cogging torque of the claw pole motor

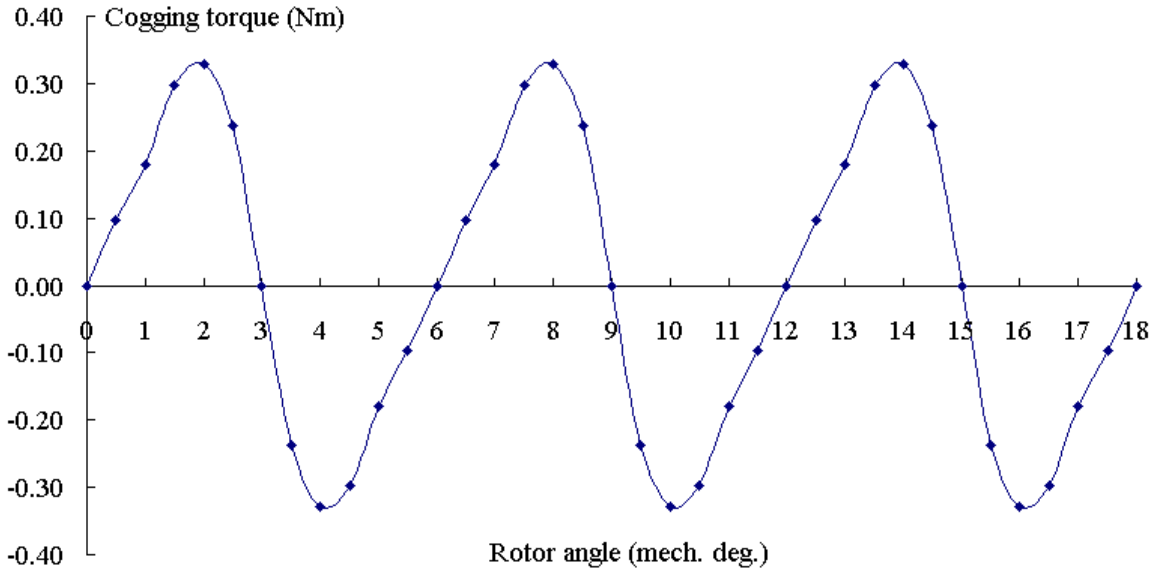

Figure 10: Measured back EMF waveforms at 1800 rpm

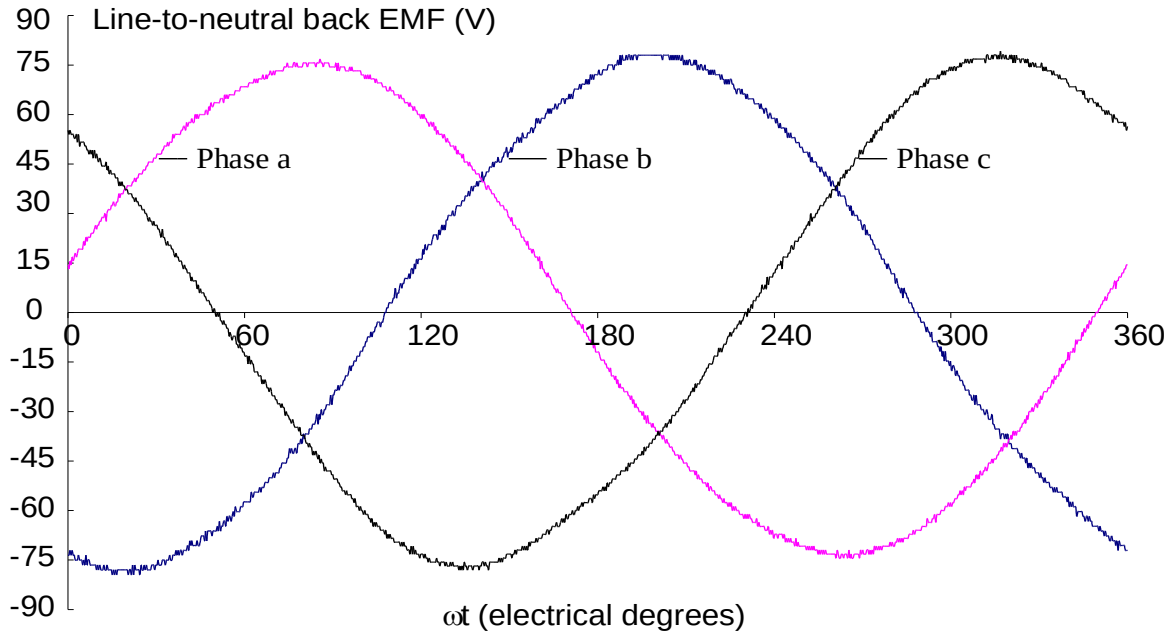

Figure 11: Curves of the speed against output torque with different DC link voltages

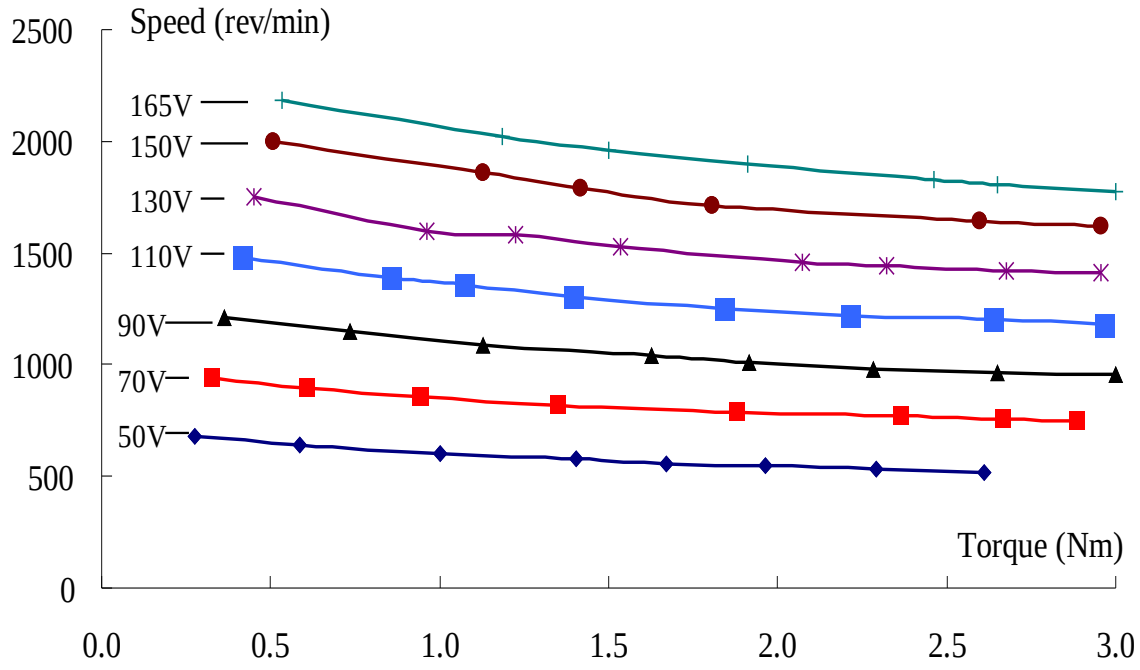

Figure 12: Inverter DC input and AC output currents against output torque

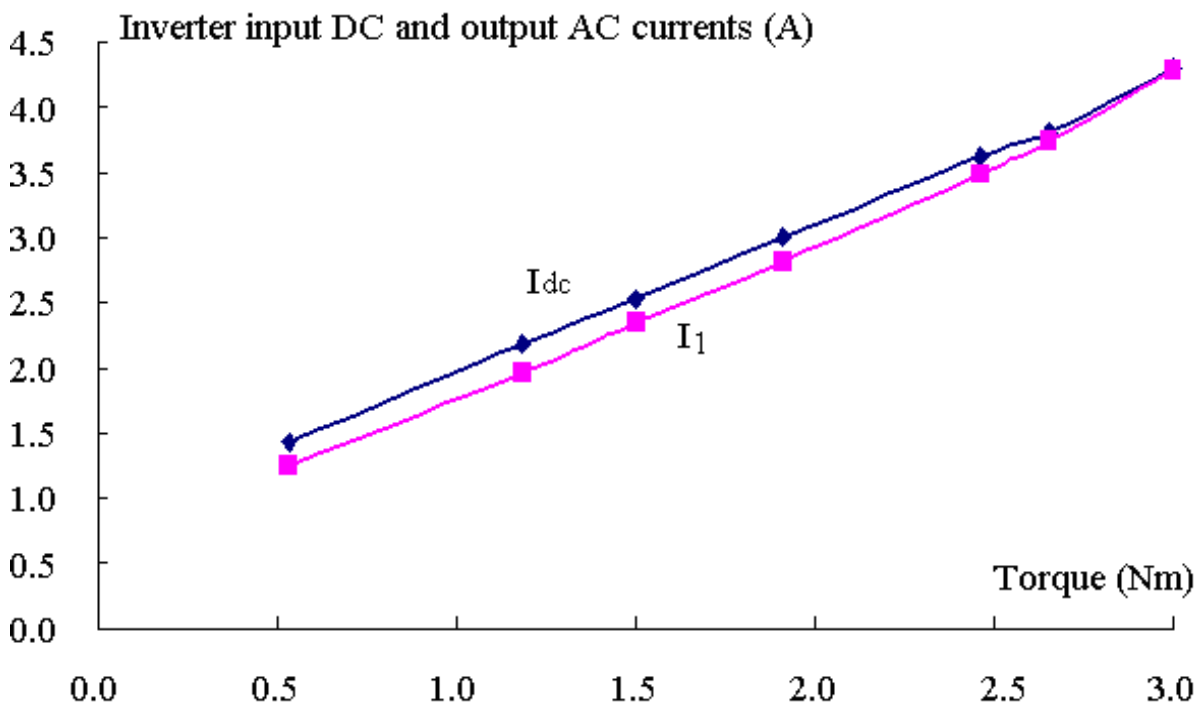

Figure 13: Curves of inverter input power, motor output power and efficiency versus output torque

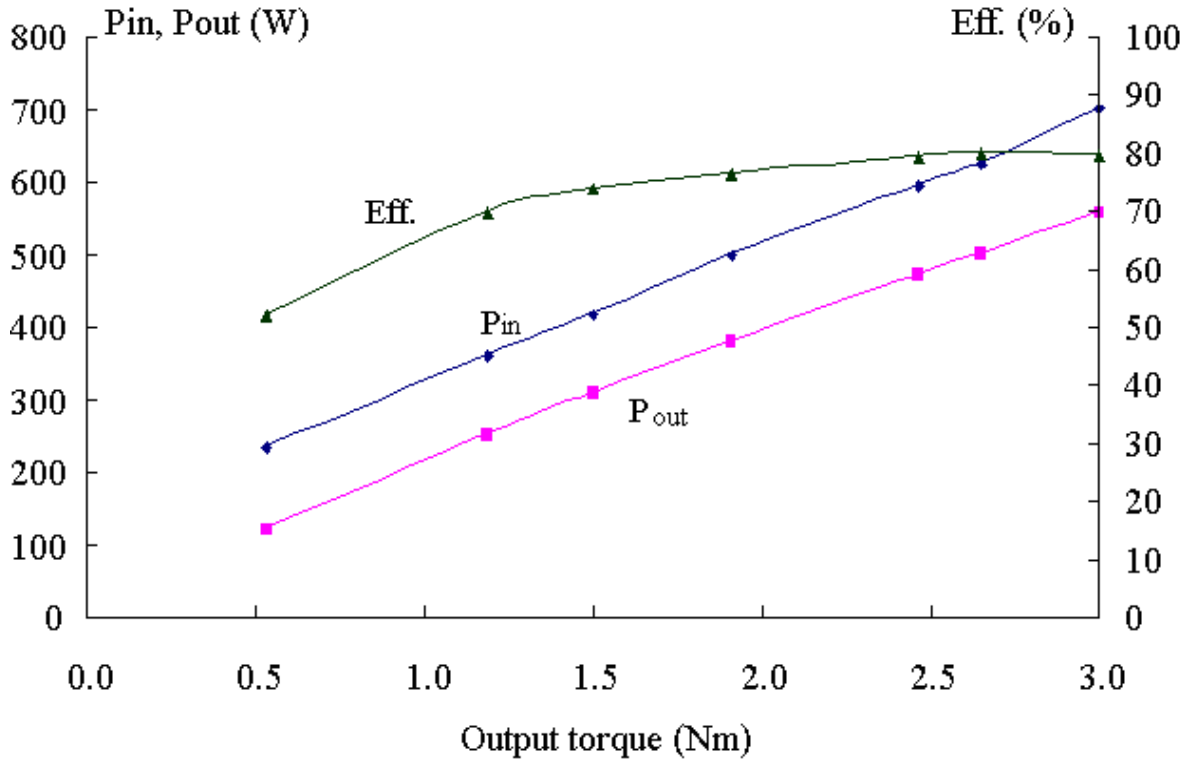

Table 1
Dimensions and major parameters

Dimensions and parameters	Quantities
Rated frequency (Hz)	300
Number of phases	3
Rated power (W)	500
Rated line-to-neutral voltage (V)	64
Rated phase current (A)	4.1
Rated speed (rev/min)	1800
Rated torque (Nm)	2.65
Rated efficiency (%)	81
Rated temperature rise (^{o}C)	75
Number of poles	20
Stator core material	SOMALOY™ 500
Stator outer radius (mm)	40
Effective stator axial length (mm)	93
Rotor outer radius (mm)	47
Rotor inner radius (mm)	41
Permanent magnets	NdFeB, Grade N30M
Number of magnets	60
Magnet dimensions	OD88 x ID82 x 15 mm arc 12^{o}
Magnetisation directions	Radially outward and inward
Main airgap length (mm)	1
Sub-airgap length* (mm)	4.2
Stator shaft material	Mild steel
Shaft outer radius (mm)	9
Number of coils	3
Coil window dimension (mm^2)	17 x 11
Number of turns	75
Number of strands	2
Diameter of copper wire (mm)	0.71
Resistance per phase at 115^{o}C (Ω)	0.302

* The sub-airgap is defined as the gap between the sides of the claw poles of the two separated pieces.

Table 2

Inductance and armature reaction in magnets

Rotor position (elec. deg.)	Self inductance per turn (μH)	Maximum B in magnets (T)
0	0.932	0.031
45	0.932	0.030
90	0.932	0.037

Table 3
Comparison of SMC and mild steel

Parameters	SMC	Mild steel
Relative permeability	130	5000 (range 1500 –10000)
Conductivity (S/m)	500 - 10000	1.12×10^7
Penetration or skin depth at 300 Hz (mm)	25.5 – 114	0.123